Transient resonance structures in electron tunneling through water

Uri Peskin, Åke Edlund, and Ilan Bar-On
Department of Chemistry, Technion-Israel Institute of Technology, Haifa 32000, Israel

Misha Galperin and Abraham Nitzan[a)]
School of Chemistry, Tel-Aviv University, Tel Aviv, Israel

(Received 21 May 1999; accepted 14 July 1999)

The mechanism of electrons tunneling through a narrow water barrier between two Pt(100) metal surfaces is studied. Assuming an adiabatic picture in which the water configuration is static on the time scale of the electron motion, the tunneling probabilities are found to increase nonmonotonically as a function of incident electron energy. A numerical investigation of single electron scattering wave functions suggests that the tunneling is enhanced by resonances, associated with molecular cavities in which the electron is trapped between repulsive oxygen cores. The lifetimes of these resonances are calculated using a novel filter diagonalization scheme, based on a converging high-order perturbative expansion of the single-electron Green's function, and are found to be of order $\leqslant 10$ fs. The possibility that transient resonance supporting structures contribute to the enhancement of tunneling through water is discussed. © *1999 American Institute of Physics*. [S0021-9606(99)70538-6]

I. INTRODUCTION

Electron transmission in and through condensed environments has been a subject of intensive studies over several decades. The most common chemical example is electron transfer between donor and acceptor molecules in solution.[1] Here the main role played by the solvent is to affect energy matching between donor and acceptor levels by thermal fluctuations. Continuum dielectric theory provides a reasonable description of this effect, however, it obviously cannot describe the effect of solvent structure on the electronic coupling itself. This deficiency becomes particularly important in electron transfer at interfaces and in electron transmission through thin molecular layers (e.g., ''underwater'' STM (scanning tunneling microscopy) experiments,[2] electron tunnel-junctions involving metal-molecular layer-metal contacts,[3] photoemission through absorbed molecular layers,[4] and electron injection into metals through molecular adsorbates[5]), where new molecular structures may appear. In transmission processes the initial and final electron states belong to continuous manifolds, so the issue of donor–acceptor energy matching becomes moot and the main effect of the molecular environment is the one it has on the electronic coupling, i.e., on the transmission probability. In a recent series of papers this issue has been investigated by evaluating numerically electron transmission probabilities through static water layer structures.[6]

An important issue raised by these previous studies[6] was the possible involvement of transient water structures that may enhance electron transmission via resonance tunneling. It was found that such resonances exist within ~1 eV below the bare vacuum barrier, however, their nature and properties were not elucidated. Here we address this issue in more detail by calculating the electron scattering wave functions. This enables us to correlate the resonant enhancement with particular water nanostructures, and to estimate the corresponding resonance lifetimes.

II. THE MODEL SYSTEM

We use the same Pt(100)–H_2O–Pt(100) model system that was studied by Benjamin *et al.* previously,[6] [a polarizable flexible simple point charge (PFSPC) potential for the water–water interaction, Pt(100) surface with water–Pt interaction taken from the work of Sphor and Heinzinger[7]]. We also use the same electron–water pseudo-potential used in Refs. 6. This potential is based on that developed by Barnett *et al.*[8] modified to include the many-body interaction associated with the water electronic polarizability of water as described in Ref. 6. The electron metal pseudo-potential is represented by a square barrier of height 5 eV. The total potential experienced by the electron is assumed to be a superposition of these electron–water and electron–metal pseudopotentials. The studies described below are done for a distance of 10 Å between the Pt walls, which accommodates three water monolayers at normal density. Water configurations are prepared by classical MD (molecular dynamics) evolution at 300 K, using minimum image periodic boundary conditions in the directions parallel to the metal walls. Overall, 197 water molecules are contained in the simulation cell, and the system was equilibrated for 200 ps before selected water configurations were studied. More details about this classical MD simulation are provided in Ref. 6(c). Following the equilibration period we have collected water configurations at intervals of 10 ps. In what follows we refer to these configurations by the corresponding time along the trajectory (e.g., the 50 ps configuration is the structure obtained 50 ps after the end of the equilibration period).

For each (static) water configuration obtained in this way a potential field for the electron motion is obtained as a su-

[a)]Electronic mail: nitzan@post.tau.ac.il

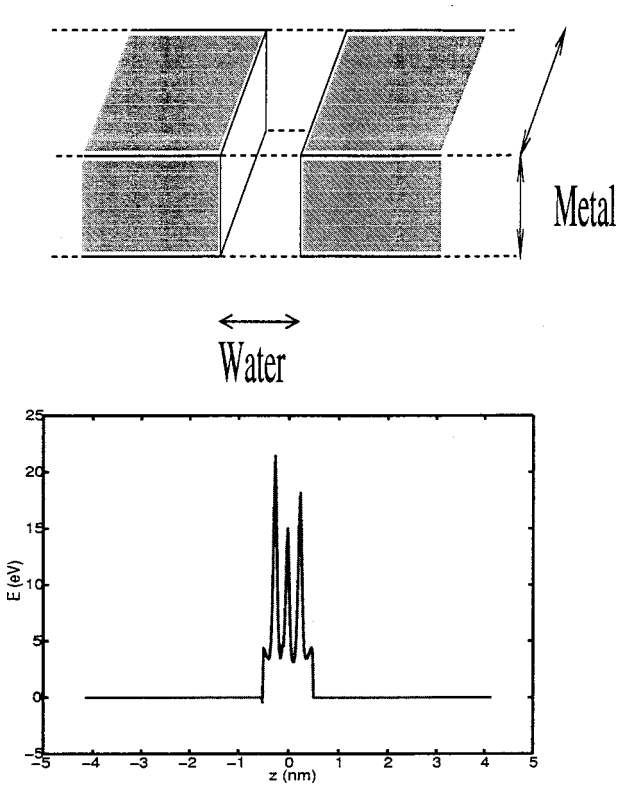

FIG. 1. Effective single electron potential. Top: The metal water–metal system. Bottom: a typical electron water interaction as a function of the tunneling z direction, averaged over the lateral (x,y) directions.

perposition of the square barrier representing the electron–metal interaction and the electron water pseudopotential. This potential is projected into a cubic grid of dimension $16\times16\times400$ with corresponding grid spacings $2.77\times2.77\times0.4$ a.u. in the (x,y,z) directions (z is the tunneling direction). The electronic problem is solved on this (23.45,23.45,84.7) Å grid using periodic boundary conditions in the x and y directions and absorbing boundary conditions in the tunneling (z) direction, as described below. A schematic view of the simulated system and the (x,y) average of the potential experienced by the electron is shown in Fig. 1.

The resulting electron tunneling probabilities through frozen water configurations are presented in Sec. III. The transmission probability displayed as a function of the incident electron energy show distinct but configuration dependent peaks below the bare (5 eV) work function. These peaks were interpreted in Refs. 6(b) as resonance tunneling features, associated with transient water structures. In Sec. IV we trace the origin of these resonances to transient nanocavities in the water structure. This assignment is made by calculating the three-dimensional electron scattering functions in the barrier regions. The resulting functions are strongly localized inside such cavities. Section V describes the calculation of the corresponding resonance eigenvalues, using a novel filter diagonalization scheme based on a high-order expansion of the Green's function. Typical resonance widths are found to be $\sim$0.05 eV, implying characteristic lifetimes $\leqslant$10 fs. Conclusions regarding the origin of the unusually low effective barrier found for electron tunneling through water, the possibility that rare fluctuations from equilibrium may contribute to this tunneling enhancement and the relevance of studies based on frozen water configurations to these processes are presented in Sec. VI.

III. THE TRANSMISSION PROBABILITY

As in Refs. 6(b)–6(d) and 9 we use the absorbing boundary condition Green's function method to evaluate the transmission probability for an incoming electron. A stationary incident electron flux is represented as a free wave perpendicular to the metal surfaces along the tunneling direction z

$$\phi_E(x,y,z) \xrightarrow{z\to-\infty} \sqrt{\frac{m_e}{k_z\hbar}}e^{ik_zz}, \tag{1}$$

The elastic transmission probability in the forward direction ($z\to\infty$) are calculated using the formulation of Miller *et al.*[9](b)

$$P(E)=\frac{2}{\hbar}\langle\phi_E|\epsilon_-G^*(E)\epsilon_+G(E)\epsilon_-|\phi_E\rangle$$

$$\equiv\frac{2}{\hbar}\langle\psi_E|\epsilon_+|\psi_E\rangle. \tag{2}$$

$G(E)$ is the approximate Green operator

$$G(E)=\frac{1}{[E-H+i\epsilon_-+i\epsilon_+]}, \tag{3}$$

where $E=(\hbar^2k_z^2)/(2m_e)$ is the incident electron energy, H is the single electron Hamiltonian

$$H=\frac{-\hbar^2}{2m_e}[\nabla_x^2+\nabla_y^2+\nabla_z^2]+V(x,y,z)\equiv H_0+V, \tag{4}$$

and $V(x,y,z)$ is the superposition of the barrier and the electron–water interaction. The approximate Green operator contains explicit boundary operators which replace the analytic limit $\epsilon\to0$. In the present work these operators were taken as a steeply rising local functions at the boundaries of the tunneling axis, which was sampled on a finite interval $-L_z/2<Z<L_z/2$

$$\epsilon_+(z)=\begin{cases}\epsilon_0\left(\dfrac{2|z|}{L_z}\right)^7; & z\geqslant0\\ 0; & z<0\end{cases}, \tag{5}$$

$$\epsilon_-(z)=\epsilon_+(-z).$$

In the calculation reported below ϵ_0 is of order 1 a.u. and the computed transmission was found to be stable with respect to the specific choice of this parameter within the desired accuracy, which implies that the absorbing operators were switched on sufficiently far from the interaction region.

The main computational task in the calculation of $P(E)$, Eq. (2), involves the evaluation of the function $\psi_E=iG(E)\epsilon_-\phi_E$. This is carried out by solving an inhomogeneous Schrödinger equation

$$[E-H+i(\epsilon_++\epsilon_-)]\psi_E=i\epsilon_-\phi_E, \tag{6}$$

on the discretized three-dimensional grid. The large ($16\times16\times400$) size of the linear system in the present applica-

tion makes it necessary to apply sparse iterative solvers. A particularly efficient solver is based on a converging high-order perturbative expansion of the Green operator

$$G(E)\psi_E=\sum_{l=1}^{k}\alpha_l(G_0(E)V)^l G_0(E)\psi_E, \tag{7}$$

where the expansion coefficients α_l are optimized for any k-order approximation by the quasi minimal residual (QMR) algorithm.[10] The zero-order Green operator is given by

$$G_0(E)=\left[E+\frac{\hbar^2}{2m_e}[\nabla_x^2+\nabla_y^2+\nabla_z^2]+i(\epsilon_+ +\epsilon_-)\right]^{-1}. \tag{8}$$

Making use of the separable structure of G_0^{-1}, the approximate Green operator can be applied in terms of a sequence of one dimensional diagonalization transformations,[9(c),9(d)]

$$G_0=U_xU_yU_z[\lambda_x+\lambda_y+\lambda_z]^{-1}U_z^{-1}U_y^{-1}U_x^{-1}, \tag{9}$$

where the diagonalization transformations are

$$\left[E+\frac{\hbar^2}{2m_e}\nabla_z^2+i(\epsilon_+ +\epsilon_-)\right]U_z=U_z\lambda_z,$$

$$\frac{\hbar^2}{2m_e}\nabla_y^2U_y=U_y\lambda_y, \tag{10}$$

$$\frac{\hbar^2}{2m_e}\nabla_x^2U_x=U_x\lambda_x.$$

This separable pre-diagonalization scheme enables the use of either low-order[6(b)–6(d)] or high-order[11] differencing schemes, or the Fourier method for a discrete representation of the kinetic-energy operators.[9](c) In the present application the Sinc-discrete variable representation of Ref. 11 was applied along the tunneling direction with absorbing boundaries, and the Fourier grid representation was used along the lateral (x,y) directions.

Figure 2 shows transmission probabilities as functions of electron incident energy, computed for several water configurations sampled from the classical equilibrium MD trajectory at the times (after the equilibration period) indicated in the caption. The resulting transmission probabilities obviously depend on the water structure. In particular, the transmission peaks seen below the bare 5 eV threshold vary in position and intensity as the water configuration evolves. It should be emphasized that with current experimental (e.g., STM) time resolutions these fluctuating structures in the transmission spectrum will average out, however, their effect is expected to be seen as an overall enhancement of the averaged transmission probability.

The appearance of these peaks in the energy dependent transmission suggests that the water structures support resonance states whose position and coupling properties vary with the water configuration. Next we confirm the resonance nature of these transmission peaks and investigate their origin in the supporting water structures.

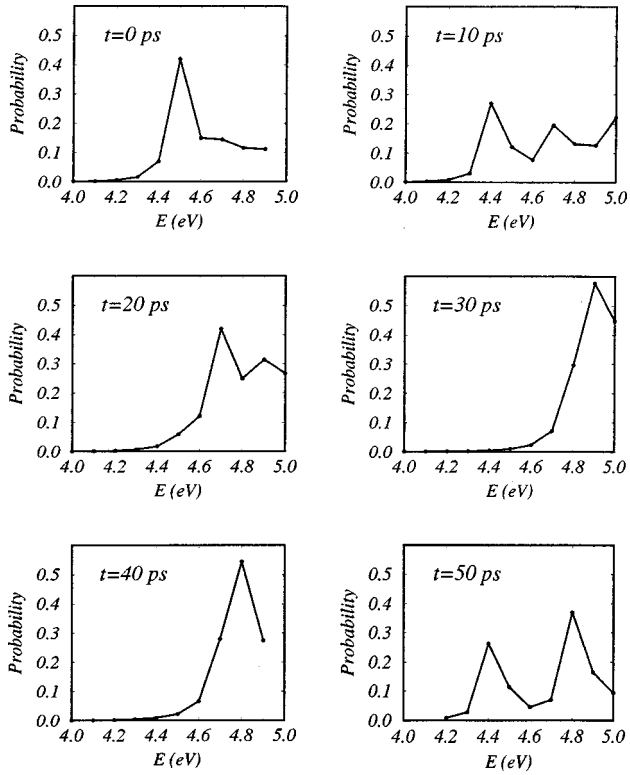

FIG. 2. Tunneling probabilities as functions of electron energy. Different lines correspond to different water configurations sampled from an equilibrium trajectory at the times (after the equilibration period) indicated in the upper left corners. The probabilities were calculated according to Eq. (2), for an electron incident in the normal (z) direction to the water layer, on a discrete grid $x_n=-22.16+2.77(n-1)$, $y_n=-22.16+2.77(n-1)$, $z_m=-80+0.4(m-1)$ a.u.; $n=1,...16$, $m=1,...400$. Absorbing boundaries [Eq. (5)] with $\epsilon_0=1$ a.u. were applied in the Z direction.

IV. THE STRUCTURAL ORIGIN OF THE TUNNELING RESONANCES

As shown above, the detailed dependence of the transmission on the incident electron energy is different for different water configurations. However, the structural origin of this dependence can not be elucidated on the basis of transmission calculations alone. In order to correlate the apparent resonances to particular water structures, detailed electron scattering wave functions (or rather probability densities) were studied for different water configurations and at different scattering energies. This analysis is based on an approximate representation of stationary electron scattering wave functions within the absorbing boundaries approximation as described above. We define this approximate scattering wave function by

$$\psi_E(x,y,z)=iG(E)\epsilon_-\phi_E(x,y,z), \tag{11}$$

where ϕ_E is the asymptotic incoming wavefunction [Eq. (1)] and $G(E)$ is defined as in Eq. (3). Equation (11) can be rewritten as an inhomogeneous Schrödinger equation

$$[E-H_0-V+i\epsilon_-+i\epsilon_+]\psi_E=i\epsilon_-\phi_E. \tag{12}$$

In the incoming flux region (i.e., $z\rightarrow-\infty$) $\psi_E(x,y,z)$ satisfies the correct incoming wave boundary conditions

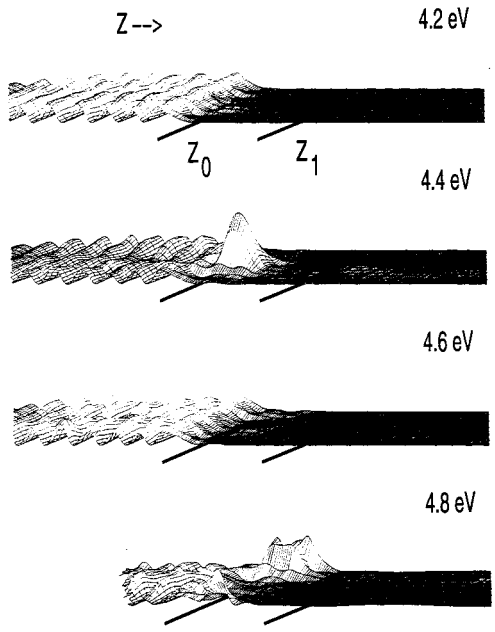

FIG. 3. Probability densities, $|\psi_E(x,y,z)|^2$, for different energies as indicated on top of each plot, for the water configuration ''$t=50$ ps'' of Fig. 2. The plots represent two dimensional cuts in the (x,z) plane for a fixed value of y ($y=2.77$ a.u.). The parameters Z_0 and Z_1 correspond to the edges of the bare barrier ($Z_0=-5$ Å, $Z_1=5$ Å).

$$\psi_E(x,y,z) \xrightarrow{z\to-\infty} \phi_E(x,y,z), \tag{13}$$

since the effective electron–water interaction vanishes inside the metal, i.e.,

$$V \xrightarrow{z\to\pm\infty} 0, \tag{14}$$

and since

$$\epsilon_+ \xrightarrow{z\to-\infty} 0, \tag{15}$$

and

$$[E-H_0]\phi_E(x,y,z)=0. \tag{16}$$

In the range of the electron water interaction the boundary operators vanish

$$\epsilon_\pm \xrightarrow{z\to0} 0, \tag{17}$$

and the inhomogeneous equation Eq. (12) reduces to the Schrödinger equation

$$[E-H_0-V]\psi_E \xrightarrow{z\to0} 0, \tag{18}$$

which implies that ψ_E approximates the exact solution ψ_E for which $[E-H_0-V]\psi_E=0$. At the positive asymptote $z\to\infty$, ϵ_-, and V vanish, while $\epsilon_+ \xrightarrow{z\to\infty} \infty$. Therefore, $\psi_E \xrightarrow{z\to\infty} 0$ unlike the exact solution. However, our focus is on the electron wave function in the water barrier and for this purpose ψ_E provides a reasonable approximation as long as ϵ_+ rises from zero sufficiently far from the electron–water interaction range.

In Fig. 3 scattering wave functions are presented for the particular water configuration which corresponds to the $t=50$ ps panel in Fig. 2, for different incident electron energies. At $E=4.2$ and $E=4.6$ eV the electron probability density peaks mostly in front of the water barrier ($z<z_0$), and the transmission through the barrier is negligible, as expected in a deep tunneling regime. A qualitatively different behavior of the probability density is found at energies 4.4 and 4.8 eV, which correspond to the peaks in the transmission probability for this configuration. The wave functions associated with these energies are localized mostly inside the water barrier (-5 Å$=z_0<z<z_1=5$ Å). A similar behavior is found for other water configurations as illustrated in Fig. 4. The correlation between the peaks in the transmission probability and the localization of the wave function inside the water barrier is indicative of a resonance tunneling mechanism, and suggests that the three-dimensional water–electron interaction potential supports quasi-bound resonance states at selected (quantized) energies.

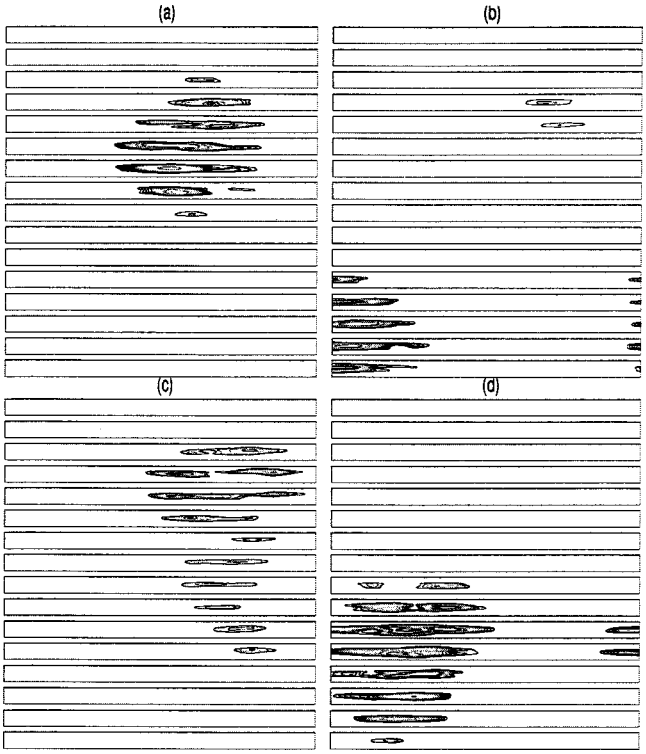

FIG. 4. Probability density contours for the transmitted electron. The different plots correspond to energies in which tunneling current is enhanced for selected water configurations that were presented in Fig. 2. (a) $t=50$ ps, $E=4.4$ eV, (b) $t=50$ ps, $E=4.8$ eV, (c) $t=40$ ps, $E=4.8$ eV, (d) $t=0$ ps, $E=4.5$ eV. The different slots in each panel are two dimensional (x,z) contour plots of the probability density, $|\psi_E(x,y_n,z)|^2$, in the water region: $x=-22.16\cdots22.16$ a.u., $z=-9.45\cdots9.45$ a.u., with $y_n=-22.16+2.77(n-1)$ a.u., $n=1,2,...,16$ from top to bottom in each panel.

The nature of these quasibound states is revealed by correlating the localized wave functions with the corresponding potential-energy surfaces of the electron–water interaction (Figs. 5 and 6). It is found that the quasibound states are localized in cavities between repulsive oxygen cores. Such cavities are generated due to the thermal disorder in water, and their lifetime is on the time scale of the intermolecular motions. Since the water density between the metal surfaces is constant, the cavities are found at any time (i.e., at any

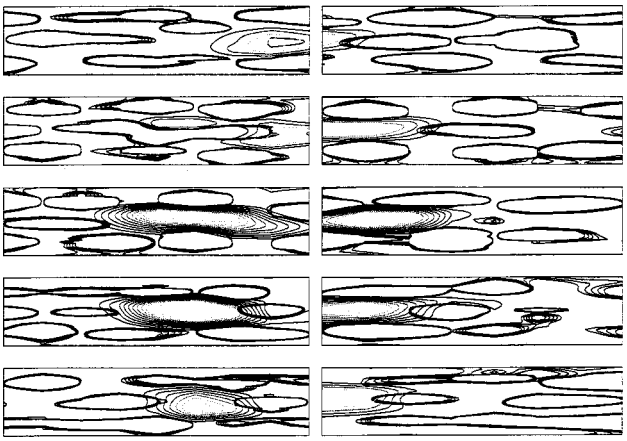

FIG. 5. Probability density $|\psi_E(x,y,z)|^2$ (the dense contour lines) for the transmitted electron in the $t=50$ ps water configuration of Fig. 2, plotted on top of the contour lines of the electron–water interaction potential at the range $3.8<V<5$ eV, for the incident energies $E=4.4$ eV (left) and $E=4.8$ eV (right) that correspond to the transmission resonance peaks seen for this configuration. The different slots in the right and left panels are *xz* contour plots in the barrier region (for details see caption to Fig. 4) for different posions y_n along the *y* axis: Left panel $n=4,5,6,7,8$; Right panel: $n=12,13,14,15,16$.

''frozen'' water configuration), but their spatial location and shape change with the time evolution of the molecular structure (see Fig. 4).

We end this section with two more observations. First, all the ''configurational holes'' that were found in the three monolayer water structures were in the middle layer, the layers adsorbed on the metal surfaces are much more ordered and less subject to disordering fluctuations. Similar holes (and similar resonances in the transmission) are found also in the ''bulk'' region of thicker water layers.[12]

Secondly, we have found that the existence of resonance supporting structural holes is surprisingly resilient to increasing water density. Adding five water molecules to our molecular system did not eliminate neither the structural holes nor the resonances supported by them, while adding nineteen molecules (density change of ~10%) did.

Finally, it should be emphasized again that because the resonance structure of the electron transmission through water strongly depends on the water configuration, no such structure is expected in experiments that monitor signals average over long $\geqslant$1 ps) times. On the other hand it is possible that the existence of these resonances causes the experimentally observed enhanced (relative to expectations) tunneling of electron in water.[2(a),2(d)] Not only does transmission increases by resonant tunneling, also the distance (thickness of the water layer) dependence may become considerably weaker than expected. We have argued elsewhere[13] that analyzing tunneling affected by resonances using simple square barrier models may lead to strongly underestimated effective barrier.

It should be kept in mind, however, that these observations are based on computation of tunneling through static water configurations. While the electron tunneling time through a simple barrier of height 1 eV (above incident energy) and width 10 Å is estimated to be ~1 fs, resonance

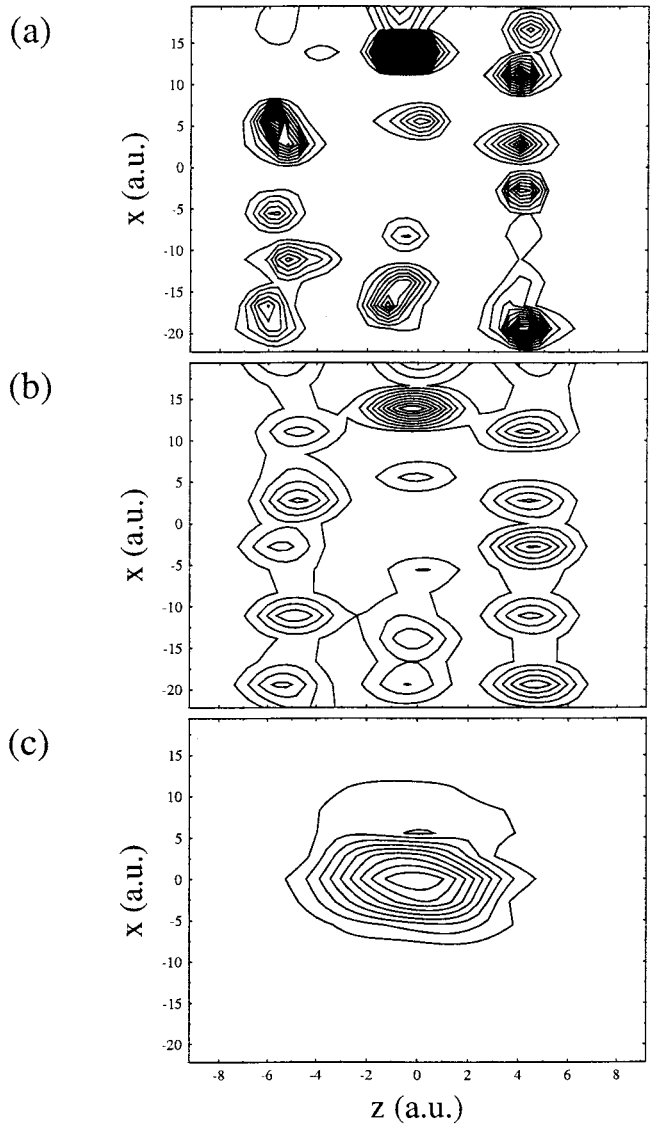

FIG. 6. Another view of the structure that give rise to the 4.4 eV resonance in the $t=50$ ps configuration (Fig. 2). (a) A contour plot of the potential, $V(x,y_n,z)$ for $n=2$ ($y_n=-19.4$ Å). (b) A contour plot of the oxygen atoms configuration on the same plane. This plot is obtained by assigning to each O atom a Gaussian, $g(r)=\exp(-((r-r_0)/\sigma)^2)$, with r_0 the center and σ the radius of the atom. (c) A contour plot of $|\psi_E(x,y,z)|^2$ in the same plane.

tunneling is associated with a characteristic delay time, for which the static picture of water may no longer be valid. It is, therefore, important to estimate the time scale associated with the resonant process. We now turn to this issue.

V. RESONANCE LIFETIMES

The increased electron transmission probability near quasibound state energies is associated with a time delay of the electron motion inside the water barrier. In this section we study the characteristic time delay for the trapped electrons. The quasibound states are associated with resonance eigenvalues of the time independent Schrödinger equation with outgoing wave (Sigert) boundary conditions. In the present treatment the boundary conditions are imposed in terms of the imaginary boundary operators along the *z* axis, given by Eq. (5), and the Schrödinger equation reads

$$[\lambda - H + i(\epsilon_+ + \epsilon_-)]\psi_\lambda = 0. \tag{19}$$

For resonance eigenvalues $\lambda = E_{\rm res} - i\Gamma/2$, where $E_{\rm res}$ is the resonance energy and $\tau = \hbar/\Gamma$ is the decay time of the trapped resonance state. In order to calculate the resonance eigenvalues that contribute to the tunneling enhancement, a filter diagonalization scheme[14] was applied. The relevant energy interval in the range $4 < E_n < 5$ eV on the real energy axis was discretized into N_E energies ($n = 1,2,...,N_E$). At each energy a Green operator was applied onto a random vector $\Re$

$$G(E_n)\Re = [E_n - H + i(\epsilon_+ + \epsilon_-)]^{-1}\Re = \phi_n, \tag{20}$$

projecting it on a vector ϕ_n close to the eigenvectors of $[H - i(\epsilon_+ + \epsilon_-)]$, with energies closest to E_n. The set of vectors $\{\phi_n\}$ are used as a basis set for a compact $(N_E \times N_E)$ discrete representation of the eigenvalue equation, whose solutions approximate the exact eigenvalues of $H - i(\epsilon_+ + \epsilon_-)$

$$\underline{\underline{\mathbf{H}}}\psi_\lambda = \lambda \underline{\underline{\mathbf{S}}}\psi_\lambda, \tag{21}$$

Where

$$\begin{aligned} \underline{\underline{H}}_{n,m} &= \langle \phi_n^* | (H - i\epsilon) | \phi_m \rangle \\ &= \langle \Re^* | G(E_n)(H - i\epsilon) G(E_m) | \Re \rangle \\ &= E_m \underline{\underline{S}}_{n,m} - \langle \phi_n^* | \Re \rangle \end{aligned} \tag{22}$$

and

$$\begin{aligned} \underline{\underline{S}}_{n,m} &= \langle \Re^* | G(E_n) G(E_m) | \Re \rangle \\ &= \begin{cases} \dfrac{\langle \phi_n^* | \Re \rangle - \langle \phi_m^* | \Re \rangle}{E_m - E_n}; & m \neq n \\ \langle \phi_n^* | \phi_n \rangle; & m = n \end{cases}. \end{aligned} \tag{23}$$

Note that since the matrix representation of $H - i(\epsilon_+ + \epsilon_-)$ is complex symmetric (non-Hermitian) the left eigenvectors are not complex conjugates of the right eigenvectors, and the complex inner product is applied.[15(a)] As one can see the construction of the generalized eigenvalue equation [Eq. (21)] requires only two sets of N_E overlap integrals $\{\langle \phi_n^* | \Re \rangle\}$ and $\{\langle \phi_n^* | \phi_n \rangle\}$, and the main computational task, i.e., the calculation of the vectors $\{\phi_n\}$ according to Eq. (20), is again done using the high-order expansion of $G(E)$ as described in Sec. III.

In Fig. 7 the complex eigenvalues of Eq. (21) are plotted for the static electron potential associated with the water configuration at $t = 50$ ps (see Fig. 2). Figures 8 and 9 below also refer to the same configuration. These eigenvalues can be classified into two groups according to the corresponding eigenvectors $\psi_\lambda(x,y,z) = \sum_{n=1}^{N_E} a_{\lambda,n}\phi_n(x,y,z)$. In the first group the densities $|\psi_\lambda|^2$ are delocalized outside the water barrier (see Fig. 8). These are continuum functions that are discretized by imposing the artificial boundary conditions $\psi_\lambda(x,y,z) \xrightarrow[z \to L_z/2]{} 0$. The other group of states includes eigenfunctions that are localized inside the water barrier (Fig. 8). These are the states associated with the resonance transmission, and are similar to the localized scattering wave functions in Fig. 3. The corresponding exact resonance states

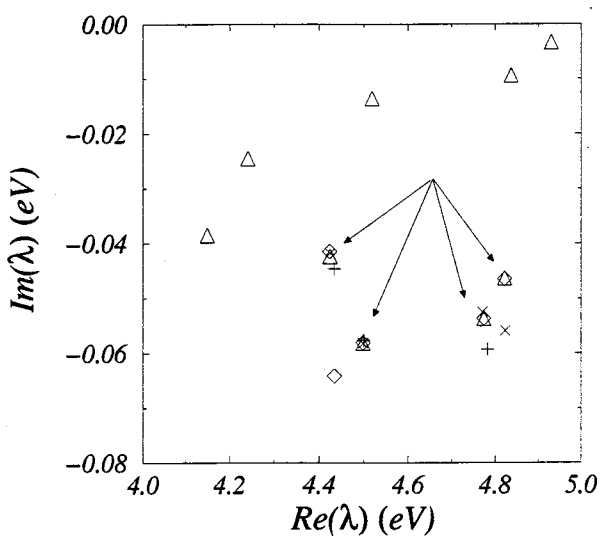

FIG. 7. Complex eigenvalues of the single electron Hamiltonian with absorbing boundary operators [water configuration $t = 50$ ps of Fig. 2; $\epsilon_0 = 2.0$ a.u. in Eq. (5)]. The pluses, crosses, diamonds, and triangles correspond to results of filter diagonalization with $N_E = 7,10,15,30$ in the energy interval $4 < E < 5$ eV. The converged eigenvalues are marked with arrows.

are associated with poles of the scattering matrix in the lower half of the complex energy plane and therefore with asymptotically diverging outgoing (Sigert) waves

$$\psi_{\lambda_{\rm res}}(x,y,z) \xrightarrow{z \to \infty} S(\lambda_{\rm res}) e^{i(\sqrt{2m_e\lambda_{\rm res}})z/\hbar}, \tag{24}$$

where the divergence ''rate,''-Im$[\sqrt{2m_e\lambda_{\rm res}}]/\hbar$ is determined by the complex pole, $\lambda_{\rm res} = \lambda_R - i\lambda_I$. When the artificial boundary operators are added to H, this divergence can be

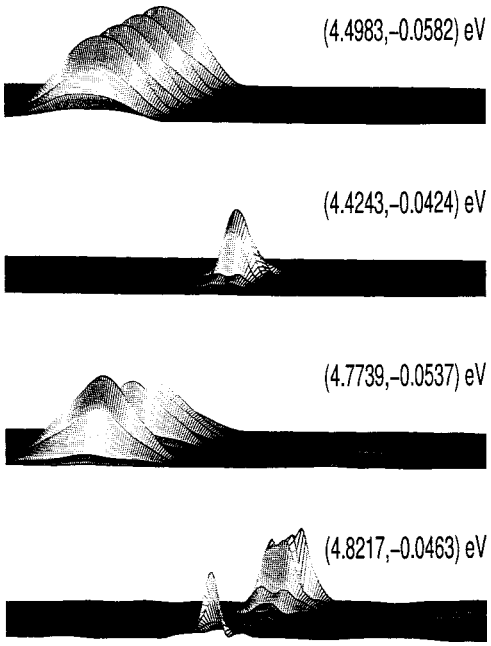

FIG. 8. Plots of the approximate eigenfunctions of $[H - i(\epsilon_+ + \epsilon_-)]$, corresponding to the converged eigenvalues of Fig. 7 ($\epsilon_0 = 2.0$ a.u.). Each plot is a cut through $|\psi_\lambda(x,y,z)|^2$ in the (x,z) plane for $y = 2.77$ a.u., using arbitrary normalization of ψ. The eigenvalues are marked on the top of each plot.

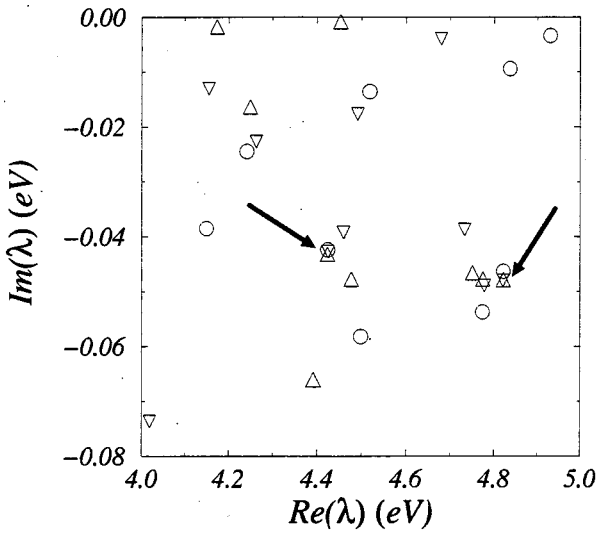

FIG. 9. Eigenvalues of $[H-i(\epsilon_+ + \epsilon_-)]$ for different absorbing boundary operators. The triangles down, triangles up, and circles correspond to $\epsilon_0 = 0.5, 1.0, 2.0$ a.u. in Eq. (5). The stable resonance eigenvalues (corresponding to the localized eigenfunctions in Fig. 8) are marked with arrows.

compensated by an asymptotic decay, provided that $\epsilon_\pm$ are sufficiently large. In this limit the resonance eigenvalues are associated with asymptotically decaying eigenfunctions of $[H-i(\epsilon_+ + \epsilon_-)]$ which satisfy the artificial boundary conditions, regardless of the specific choice of the boundary operators. This is illustrated in Fig. 9, in which the spectrum of $[H-i(\epsilon_+ + \epsilon_-)]$ is plotted for different choices of ϵ_0, where the stable numerical eigenvalues correspond to the localized resonance wave functions. A similar stability phenomenon is found in other methods for calculations of resonance eigenvalues such as the complex coordinate method[15(a)] and the box-stabilization method.[15(b)]

This numerical procedure which is a sequence of filter diagonalizations with different choices of $i\epsilon_\pm$, enables us to obtain resonance energies and widths for different water configurations. Characteristic results are presented in Table I for two configurations, each one supporting two resonance states.

The resonance lifetimes found are typically less than 10 fs. This time is considerably longer than that estimated for tunneling away from resonance. Still, it is short relative to the solvation response of the water environment. The fast, inertial component in the solvation dynamics of a charged species in water has been estimated by computer simulations to be 20–30 fs,[16] but recent experimental results by Barbara and co-workers[17] suggest that the simulations may have overestimated the solvation rate by at least a factor of 2. It should be emphasized that even though these timescales look favorably consistent with our static water approximation, the time scale separation is not large enough to exclude possible deviations from the adiabatic picture due to coupling to intermolecular water motions on the time scale of the electron delay. In this regard, it should be kept in mind that the period of OH stretch modes in water is of the same order as the resonance lifetimes found here. A conclusive determination of the relevance of our observations to the electron tunneling enhancement in water requires a better accounting for the role played by the water dynamics in the transmission process.

TABLE I. Resonance eigenvalues and the corresponding resonance lifetimes found for the configurations ''$t=0$'' and ''$t=50$ ps'' of Fig. 2.

Configurations	Resonance energy (eV)	Decay time (fs)
0 ps	(4.5029, −0.0541)	6
0 ps	(4.6987, −0.0545)	6
50 ps	(4.4243, −0.0424)	7.6
50 ps	(4.8217, 0.0463)	7

VI. CONCLUSIONS AND OUTLOOK

In Secs. II–IV we have discussed the possible role played by structural cavities in the water structure, that were found to support negative energy states in the range up to 1 eV below vacuum energy. We found that such structural cavities naturally exist in the water structure between the two metal electrodes, and are in fact quite resilient to density fluctuations of magnitude expected in this noncompressible fluid. We have argued that the tunneling enhancement, as well as the nonmonotonous distance dependence of the tunneling rate associated with these resonance states may contribute to the unusually low effective barrier for electron tunneling observed in recent ''underwater'' STM experiments. The possible role of resonance tunneling in electron transmission through water has been suggested before by Halbritter and co-workers,[18] however, the resonance found in the present work are very different than those suggested by these authors.

The observation that electron tunneling through water may be enhanced by special tunneling structures raises the questions that other structures caused by rare fluctuations, not observables in short time simulations of finite systems, may contribute significantly to the transmission probability. This possibility exists in principle because far below the barrier resonant tunneling can be enhanced by many orders of magnitudes relative to the nonresonant process, therefore, even rare configurations supporting such resonances may in principle dominate the transmission. The Appendix demonstrates this possibility for a particular example.

The main shortcoming of the present discussion is the use of static water configurations in the calculation of resonance tunneling. We have shown that the lifetimes of the cavity resonances discussed above is about an order of magnitude shorter than the characteristic time for water rearrangement about an electron moving in its interior. For the rarer resonance structures discussed in the Appendix, the resonance lifetime in the cavity and the cavity relaxation time itself are of the same order of magnitude. Clearly, a procedure that takes into account the water motion on the time scale of this resonance is needed for a conclusive argument.

ACKNOWLEDGMENTS

This research was supported by the Israel Ministry of Science, the Israel Science foundation, the USA-Israel Bina-

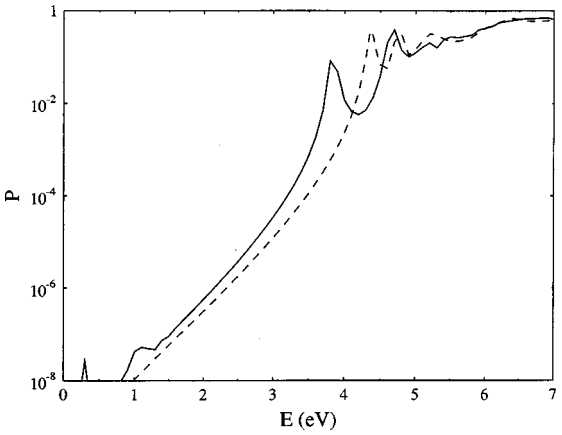

FIG. 10. Solid line: Transmission probability vs incident electron energy for the configuration with an artificially induced polarization hole (see text). For comparison, the dashed line shows the transmission probability associated one of the neutral water configurations from the run shown in Fig. 2.

tional Science Foundation and the fund for the promotion of research at the Technion. U.P. is a member of the Lise Meitner-Minerva Center for Computational Quantum Chemistry.

APPENDIX

Here we speculate on the possibility that rare molecular structures which are hard to come by in ordinary MD simulations can contribute significantly to electron tunneling by supporting resonances that give rise to strongly enhanced tunneling. As a demonstration of this possibility we consider an artificially prepared structure: Water configuration that will be in equilibrium with an anion of a chlorine anion size (radius$=1.75$ Å) carrying a charge $q=-0.2e$. Such a configuration is sampled from an equilibrium trajectory in a system (the same water layer system between the two Pt walls considered above) which contains this artificial ion in the center $(z=0)$ between the two walls. The ion is then removed for the next stage of the calculation. This stage is a computation of the transmission properties of this (static) artificial structure. The resulting transmission vs incident energy plot shows a new resonance peak at $E=3.8$ eV, below the vacuum barrier of 5 eV. At the peak energy the transmission is enhanced by a factor of ~ 500 relative to the previously studied equilibrium configurations (see Fig. 10).

Consider now the probability that such a ''polarization bubble'' would form as a spontaneous fluctuation in the equilibrium water layer. This probability is given by $P_b=\exp[-\Delta F/k_BT]$, where ΔF is the free energy change associated with this fluctuation, i.e., the reversible work required from an external force to create this bubble, T is the temperature and k_B—the Boltzmann constant.

A rough estimate of ΔF can be obtained from continuum dielectric theory as follows: The free energy gained by introducing an ion of charge q and radius R into the solvent of dielectric constant ϵ is (the Born solvation energy)

$$W_{\mathrm{Born}}=\frac{q^2}{2R}\left(\frac{1}{\epsilon}-1\right). \tag{A1}$$

This energy can be viewed as consisting of two contributions: W_1, the interaction of the ion with the polarization induced in the surrounding solvent, and W_2, the energy needed to build this polarization. W_1 is given by the product $q\times V_{\mathrm{solvent}}$ where V_{solvent} is the potential induced by the solvent at the ion's position. From $V_{\mathrm{solvent}}+(q/R)=(q/\epsilon R)$ we find $W_1=qV_{\mathrm{solvent}}=q^2/R(1/\epsilon-1)$.
Consequently

$$\Delta F=W_2=W_{\mathrm{Born}}-W_1=\frac{q^2}{2R}\left(\frac{1}{\epsilon}\right). \tag{A2}$$

When the polarization structure is prepared in an electrolyte layer of thickness L, ΔF is smaller, given by

$$\Delta F=\frac{q^2}{2}\left(1-\frac{1}{\epsilon}\right)\left[\frac{1}{R}-\frac{1}{4d}-\frac{1}{4(L-d)}\right]. \tag{A3}$$

Where d is the distance of the charge center from the layer surface. Using $R=1.75$ Å, $L=1.75$ Å, $d=L/2$, $q=-0.2e$, and $T=300$ K, we get $P_b\sim 0.009$.

A more rigorous value for ΔG can be obtained from the numerical simulations, using

$$\Delta F=2\int_0^q dq'\,q'\langle V\rangle_{q'}-q\langle V\rangle_q. \tag{A4}$$

Where the instead of using $\langle V\rangle_q=(q/R)((1/\epsilon)-1)$ for the solvent potential at the ion as before, we evaluate $\langle V\rangle_q$ from the numerical simulations. This calculation is considerably simplified if we assume that the solvent response $\langle V\rangle_q$ depends linearly on q, i.e., $\langle V\rangle_q=\alpha q$, whence

$$\Delta F=\frac{1}{2}\alpha q^2, \tag{A5}$$

α is easily obtained from the numerical simulation of the water layer between the two metal walls (which also confirm the linearly assumption), yielding $P_b\cong 0.004$, in a reasonable agreement with the continuum dielectric theory result. The product of the resulting P_b and the associated resonance enhancement factor 500 is larger than 1, indicating that it is possible for the fluctuation considered to contribute a modest enhancement to the tunneling probability.

Calculation of the lifetime of the resonance associated with the structure considered again lead to $\tau\sim 10$ fs. Molecular-dynamics simulations show that the lifetime of the polarization bubble considered above is of the same order of magnitude. We conclude that in this case the time scale separation is not large enough to validate unequivocally the estimates based on tunneling through static water configurations. Further work is needed in order to assess the possible influence or rare structural fluctuations in the solvent on electron transmission.

Obviously this naive calculation should not be taken as evidence that fluctuations of the type considered contribute significantly to the transmission process. Rather, it indicates that the possibility of electron tunneling affected by rare structural fluctuation cannot be ruled out.

[1] See, e.g., A. M. Kuznetsov, *Charge transfer in Physics, Chemistry and Biology* (Gordon and Breach, New York, 1995).
[2] (a) R. Christoph, H. Siegenthaler, H. Rohrer, and W. Wiese, Electrochim.

Acta **34**, 1011 (1989); (b) M. Bingelli, D. Carnal, R. Nyffenegger, H. Siegenthaler, R. Christoph, and H. Rohrer, J. Vac. Sci. Technol. B **9**, 1985 (1991); For later work see (c) J. Pan, T. W. Jing, and S. M. Lindsay, J. Chem. Phys. **98**, 4205 (1994); (d) Y. A. Hong, J. R. Hahn, and H. Kang, *ibid.* **108**, 4367 (1998); J. R. Hahn, Y. A. Hong, and H. Kang, Appl. Phys. **A66**, S467 (1998), and references therein.

[3] See, e.g., M. A. Reed, C. Zhou, C. Muller, T. P. Burgin, and J. M. Tour, Science **278**, 252 (1997), and references therein.

[4] (a) T. L. Gilton, C. P. Dehnbostel, and J. P. Cowin, J. Chem. Phys. **91**, 1937 (1937); (b) S. K. Jo and J. M. White, *ibid.* **94**, 5761 (1991); (c) R. Naaman, R. Haran, A. Nitzan, D. Evans, and M. Galperin, J. Phys. Chem. B **102**, 3658 (1998), and references therein.

[5] L. Sanche, Scanning Microsc. **9**, 619 (1995).

[6] (a) A. Mosyak, A. Nitzan, and R. Kosloff, J. Chem. Phys. **104**, 1549 (1996); (b) A. Mosyak, P. Graf, I. Benjamin, and A. Nitzan, J. Phys. Chem. A **101**, 429 (1997); (c) I. Benjamin, D. Evans, and A. Nitzan, J. Phys. Chem. **106**, 6647 (1997); (d) I. Benjamin, D. Evans, and A. Nitzan, J. Chem. Phys. **106**, 1291 (1997).

[7] E. Spohr and K. Heinzinger, Ber. Bunsenges. Phys. Chem. **92**, 1358 (1988); E. Spohr, J. Phys. Chem. **93**, 6171 (1989).

[8] R. N. Barnett, U. Landmann, and C. L. Cleveland, J. Chem. Phys. **88**, 4421 (1988).

[9] (a) D. Neuhauser, Chem. Phys. Lett. **200**, 7836 (1990); D. Neuhauser and M. Baer, J. Chem. Phys. **92**, 3419 (1990); (b) T. Seidemann and W. H. Miller, *ibid.* **96**, 4412 (1992); W. H. Thompson and W. H. Miller, Chem. Phys. Lett. **206**, 123 (1993); U. Peskin and W. H. Miller, J. Chem. Phys. **102**, 4084 (1995); (c) U. Peskin, W. H. Miller, and A. Edlund, *ibid.* **103**, 10030 (1995); (d) A. Edlund, I. Vorobeichick, and U. Peskin, J. Comput. Phys. **138**, 788 (1997); A. Edlund and U. Peskin, Int. J. Quantum Chem. **69**, 167 (1998).

[10] R. W. Freund and N. Nachtigal, Numer. Math. **60**, 315 (1991).

[11] D. T. Colbert and W. H. Miller, J. Chem. Phys. **96(3)**, 1982 (1992).

[12] M. Galperin, A. Nitzan, and I. Benjamin (unpublished results).

[13] A. Nitzan and I. Benjamin, Acct. Chem. Res.

[14] V. A. Mandelshtam and H. S. Taylor, J. Chem. Phys. **103**, 2903 (1995); V. A. Mandelshtam, H. S. Taylor, and W. H. Miller, *ibid.* **105**, 496 (1996).

[15] (a) N. Moiseyev, Phys. Rep. **302**, 212 (1998); (b) V. A. Mandelshtam, T. R. Ravuri, and H. S. Taylor, Phys. Rev. Lett. **70**, 1932 (1993); V. A. Mandelshtam and H. S. Taylor, J. Chem. Phys. **99**, 222 (1993).

[16] (a) B. J. Schwartz and P. J. Rossky, J. Chem. Phys. **101**, 6902 (1994); (b) R. B. Barnett, U. Landman, and A. Nitzan, *ibid.* **90**, 4413 (1989).

[17] K. Yokoyama, C. Silva, D. H. Son, P. Walhout, and P. F. Barbara, J. Phys. Chem. **102**, 6957 (1998).

[18] J. Halbritter, G. Repphun, S. Vinzelberg, G. Staikov, and W. J. Lorentz, Electrochim. Acta **40**, 1385 (1995); G. Repphun and J. Halbritter, J. Vac. Sci. Technol. A **13**, 1693 (1995). Obviously, this statement depends on one's definition of the ''dipole resonances'' suggested by Halbritter and co-workers: An electron confined between the repulsive cores of water oxygen atoms certainly constitutes a dipolar/multipolar entity. We thank Prof. Halbritter for this remark.